Journal of Neuroscience Methods 353 (2021) 109089

Contents lists available at ScienceDirect

Journal of Neuroscience Methods

journal homepage: www.elsevier.com/locate/jneumeth

Use of common average reference and large-Laplacian spatial-filters enhances EEG signal-to-noise ratios in intrinsic sensorimotor activity

Shohei Tsuchimoto [a,b], Shuka Shibusawa [c,d,e], Seitaro Iwama [a], Masaaki Hayashi [a], Kohei Okuyama [f], Nobuaki Mizuguchi [a,g], Kenji Kato [h], Junichi Ushiba [i,*]

[a] School of Fundamental Science and Technology, Graduate School of Keio University, Kanagawa, 223-8522, Japan
[b] Division of System Neuroscience, National Institute for Physiological Sciences, Aichi, 444-8585, Japan
[c] Graduate School of Frontier Biosciences, Osaka University, Osaka, 565-0871, Japan
[d] National Institute of Information and Communications Technology, Center for Information and Neural Networks, Osaka, 565-0871, Japan
[e] Japan Society for the Promotion of Science, Tokyo, 102-0083, Japan
[f] Department of Rehabilitation Medicine, Keio University School of Medicine, Tokyo, 160-8582, Japan
[g] Research Organization of Science and Technology, Ritsumeikan University, Shiga, 525-8577, Japan
[h] Center of Assistive Robotics and Rehabilitation for Longevity and Good Health, National Center for Geriatrics and Gerontology, Aichi, 474-8511, Japan
[i] Department of Biosciences and Informatics, Faculty of Science and Technology, Keio University, Kanagawa, 223-8522, Japan

ARTICLE INFO

Keywords:
Sensorimotor activity
Resting-state
EEG-fMRI simultaneous recording
Mu rhythm
EEG sensorimotor rhythm

ABSTRACT

Background: Oscillations in the resting-state scalp electroencephalogram (EEG) represent various intrinsic brain activities. One of the characteristic EEG oscillations is the sensorimotor rhythm (SMR)—with its arch-shaped waveform in alpha- and betabands—that reflect sensorimotor activity. The representation of sensorimotor activity by the SMR depends on the signal-to-noise ratio achieved by EEG spatial filters.
New method: We employed simultaneous recording of EEG and functional magnetic resonance imaging, and 10-min resting-state brain activities were recorded in 19 healthy volunteers. To compare the EEG spatial-filtering methods commonly used for extracting sensorimotor cortical activities, we assessed nine different spatial-filters: a default reference of EEG amplifier system, a common average reference (CAR), small-, middle- and large-Laplacian filters, and four types of bipolar manners (C3-Cz, C3-F3, C3-P3, and C3-T7). We identified the brain region that correlated with the EEG-SMR power obtained after each spatial-filtering method was applied. Subsequently, we calculated the proportion of the significant voxels in the sensorimotor cortex as well as the sensorimotor occupancy in all significant regions to examine the sensitivity and specificity of each spatial-filter.
Results: The CAR and large-Laplacian spatial-filters were superior at improving the signal-to-noise ratios for extracting sensorimotor activity from the EEG-SMR signal.
Comparison with existing methods: Our results are consistent with the spatial-filter selection to extract task-dependent activation for better control of EEG-SMR-based interventions. Our approach has the potential to identify the optimal spatial-filter for EEG-SMR.
Conclusions: Evaluating spatial-filters for extracting spontaneous sensorimotor activity from the EEG is a useful procedure for constructing more effective EEG-SMR-based interventions.

1. Introduction

Recently, there has been an increased interest in methods aimed at restoring lost functions in those with motor and vocal impairments using brain-computer interfaces (BCIs) or brain-machine interfaces, in which brain activity is often recorded by scalp electroencephalography (EEG) (Sitaram et al., 2017; Ushiba and Soekadar, 2016). BCI systems commonly use EEG and are thus more economical and practically feasible than other devices for measuring brain function, such as functional magnetic resonance imaging (fMRI) or magnetoencephalography, and positron emission tomography. However, its use has not yet been established for reliable detection of 'sensorimotor biomarkers', which are specific to neural activity and are sensitively predictive of participants' motor intention and actions. Electrical or magnetic field activity

* Corresponding author.
E-mail address: ushiba@bio.keio.ac.jp (J. Ushiba).

https://doi.org/10.1016/j.jneumeth.2021.109089
Received 10 July 2020; Received in revised form 18 December 2020; Accepted 21 January 2021
Available online 27 January 2021

recorded over the sensorimotor cortex is often characterized by arc-shaped mu-rhythm and beta-rhythm typically oscillating at a frequency of alpha-band (7−11 Hz) and beta-band (12−30 Hz) and termed as the sensorimotor rhythm (SMR) (Kozelka and Pedley, 1990). The EEG-SMR can be recorded by an electrode set over the sensorimotor cortex or pericentral cortex (Pfurtscheller and Aranibar, 1977). The brain activity associated with the EEG-SMR components was originally studied via task conditions (Neuper et al., 2006; Pfurtscheller et al., 2006; Ritter et al., 2009). The patterns of the intrinsic oscillationsduring task-free or resting-state conditions were recently proposed to be monitoring/predictive biomarkers of motor learning or recovery from neurophysiological diseases (Carter et al., 2010; Drysdale et al., 2017; Vahdat et al., 2011). Spontaneous neural activity reflects a history of task-dependent activation and is regarded as a robust neural trace reflecting experiential modifications (Power et al., 2011; Tsuchimoto et al., 2019). Therefore, there is an increasing interest in studying intrinsic SMR oscillations related to sensorimotor function (Tsuchimoto et al., 2017; Yin et al., 2016).

Due to the conductive nature of the scalp, EEG recoding data include various signal and noise components; spatial filters are often used to suppress spatial noise and to extract the EEG-SMR signal (Blankertz et al., 2008). For example, electrodes in the Laplacian montage average the signals of the adjacent four electrodes around a single electrode (the C3 in the case of sensorimotor activity), leading to the extraction of locally recorded brain activity with an approximate spatial second derivative (McFarland et al., 1997). This Laplacian montage method is one of the spatial high-pass filters that functions by refocusing the sensitivity characteristic of the EEG electrodes to a small volume below each electrode, thus eliminating the intermixing with brain currents from other regions (Hjorth, 1991). On the other hand, if the electrical signals or potentials of neural origins were distributed on a large scale covering multiple electrodes, application of the Laplacian montage filter may cause loss of activity amplitudes from those widespread signals or potentials. Another existing spatial-filtering method is to use the reference of an average of recording data from whole-brain electrodes (Common average reference, CAR). Mcfarland and his colleagues (1997) examined several spatial filters for EEG-SMR localized around the sensorimotor cortex, and reported that both the large-Laplacian montage and the CAR spatial-filter were sufficient to extract the cortical potentials of sensorimotor cortical activities that are modulated with the user's intention. In contrast, to assess the EEG-SMR in clinical neurophysiology, the EEG signal is usually obtained with bipolar electrodes, referencing the electrode located at C3 (closest to the sensorimotor cortex in the left hemisphere) to another electrode separated >20 mm anteriorly or posteriorly (Benbadis, 2005; Kozelka and Pedley, 1990). Because the EEG-SMR signal is assessed by analyzing features of its waveforms and discharges, including amplitude, duration, and morphology, it is important to capture these signals with high sensitivity to facilitate accurate diagnosis (Ramoser et al., 2000).

Although each EEG-SMR spatial-filtering method has been used empirically in particular studies, it remains unclear as to which of these methods results in the most accurate reflection of sensorimotor cortical activity. The recording of EEG signals is compounded by noise and other activity, due to the electrically conductive character of scalp or function-structure associations of brain network activity (Moon et al., 2017). Moreover, the EEG components not only reflect the electrode closest to the cortical activity, but also the subcortical and other regional activities (Krishnaswamy et al., 2017; Seeber et al., 2019; Zumer et al., 2014). Therefore, multimodal brain recording such as fMRI, in addition to EEG recording, is required to understand the brain activity interplay of EEG components, and to better comprehend their spatiotemporal biological significance (Goldman et al., 2000; Ritter and Villringer, 2006).

We analyzed EEG-fMRI data to identify the brain region that correlated with EEG-SMR obtained after the application of several spatial-filtering methods. We assessed the sensitivity and specificity of the various spatial-filtering methods by evaluating the relationship of the EEG-SMR signals extracted after various spatial filters with spontaneous neural activities estimated by whole-brain blood oxygen level-dependent (BOLD) signal of fMRI.

2. Methods

2.1. Participants

The present study reanalyzed data previously acquired for a different research purpose (Tsuchimoto et al., 2017). In that particular study, 19 healthy participants (13 male, 6 female, aged between 21–25 years) were recruited for a simultaneous EEG-fMRI recording study. None of the participants had any known neurological history. The experimental procedures were explained to the participants, and all participants provided written informed consent. The experimental procedures were approved by local ethics committees at Keio University Faculty of Science and Technology Bioethics Committee (No. 25−32).

2.2. Data acquisition and preprocessing

The details of EEG and fMRI data acquisition has been described in the previous study (Tsuchimoto et al., 2017), and summarized here. The data-set was acquired via fMRI scans along with EEG recording during a 10-min period in the eyes-open resting state to avoid the influence of the occipital alpha rhythm. The EEG signals were recorded with an MR-compatible amplifier (BrainAmp MR plus, Brain Products GmbH, Germany) and a 63-channel EEG electrode cap with an electrocardiogram (ECG) channel (BrainCap MR, Brain Products GmbH, Germany). The electrodes were placed according to the modified International 10−10 system (Jurcak et al., 2007). The AFz electrode was adopted as a ground electrode and the mid-front (FCz) electrode was adopted as a reference electrode, which are the default locations in the BrainAmp system. The ECG electrode was placed on the participants' backs and was used to subsequently correct ballistocardiographic artifacts in the EEG signals. The impedance of all electrodes was kept below 5 kΩ. The EEG signal was sampled at 5 kHz and filtered with a bandpass filter between 0.1 and 2500 Hz using the Brain Vision Recorder (Brain Products GmbH, Germany). Preprocessing was performed with Brain Vision Analyzer 2.0 (Brain Products GmbH, Germany), and artifacts derived from gradient and ballistocardiogram in the EEG signals were corrected (Allen et al., 2000). After artifact correction, the EEG signal was filtered with a bandpass filter (3−70 Hz) and a notch filter (50 Hz), and subsequently resampled at 250 Hz.

fMRI data were acquired on a 1.5-T MR scanner (Signa Excite, GE Healthcare, United Kingdom). The scan parameters were as follows: TR = 3000 ms; TE = 40 ms; flip angle = 70 degrees; voxel size = 3.75 mm × 3.75 mm × 4.0 mm; 30 axial slices with no gap, 200 scans). A 10-MHz master synthesizer of the MRI scanner was synchronized with the EEG amplifier system clock via a SyncBox device (Brain Products GmbH, Germany). The fMRI data were preprocessed with Statistical Parametric Mapping (SPM12, Wellcome Department of Imaging Neuroscience, London, England; http://www.fil.ion.ucl.ac.uk/spm) on MATLAB (MathWorks, Natick, Massachusetts, United States), and FMRI Expert Analysis Tool (FEAT version 6.00, http://fsl.fmrib.ox.ac.uk/fsl/fslwiki/FEAT), which is part of the FMRIB Software Library (FSL, FMRIB Analysis Group, Oxford, England; www.fmrib.ox.ac.uk/fsl). After slice-timing correction, we used ICA-AROMA (Independent Component Analysis - Automatic Removal of Motion Artifacts, https://github.com/maartenmennes/ICA-AROMA) to remove motion-related artifacts from the individual resting-state data. Because resting-state functional MRI is particularly sensitive to motion artifacts (Power et al., 2012), the independent components that were classified as motion-related were regressed out of the data. Thereafter, each volume was normalized according to the Montreal Neurological Institute template and was resampled to 2 mm cubic voxels. Compensating for imperfect registration in spatial normalization across participants and for relaxing the

statistical threshold reducing the number of independent comparisons, the normalized volumes were spatially smoothed with an isotropic Gaussian kernel (full width at half maximum, FWHM = 4 mm), and passed through a 0.0078 Hz high-pass temporal filter.

2.3. Data analyses

We focused on the following nine spatial-filtering methods referencing the C3 electrode to the other electrodes: 1) a default reference of the BrainAmp system (FCz), 2) CAR, 3) small-, 4) middle- and 5) large-Laplacian montages, and 6–9) four types of bipolar references (C3-Cz, C3-F3, C3-P3, and C3-T7) (see also Fig. 2, left column). Each spatial-filtering method was applied as a re-reference. EEG signals were segmented into successive 1-s window with no overlap, and a fast Fourier transform with a Hanning window was applied to each segment. Subsequently, the EEG-SMR power time course was obtained by averaging the powers in each frequency band (alpha: 7−11 Hz, beta1: 12−16 Hz, beta2:17−21 Hz, beta3: 22−30 Hz) (Arroyo et al., 1993; Rangaswamy et al., 2004, 2002; Ritter et al., 2009). For each spatial-filtering method, the median of the temporal fluctuations was calculated after averaging the power density spectrum across each frequency band (Fig. 1).

When performing correlation analyses between fMRI signals and EEG-SMR power time courses, we followed a previous study with the simultaneous EEG-fMRI recording (Huster et al., 2012). The EEG-SMR power time course was convolved with the canonical hemodynamic response function to model the BOLD signal representing the EEG-SMR power modulation. The convolved EEG-SMR power time course was then down-sampled with the data point sampled at the reference of the fMRI slice timing correction; that is, one data point was sampled in the middle of every TR, corresponding to the fMRI slice-timing correction. To identify the brain regions that correlated with the EEG-SMR power time course, we used general linear model (GLM) analysis. To avoid multicollinearity, the GLM model was created in each frequency-band and each spatial-filtering method. In the GLM model, the cerebrospinal fluid (CSF) signal was used as a nuisance variable to remove non-neural noise originating from cardiac effects and respiration. The CSF time series were obtained by averaging the signals over all voxels within

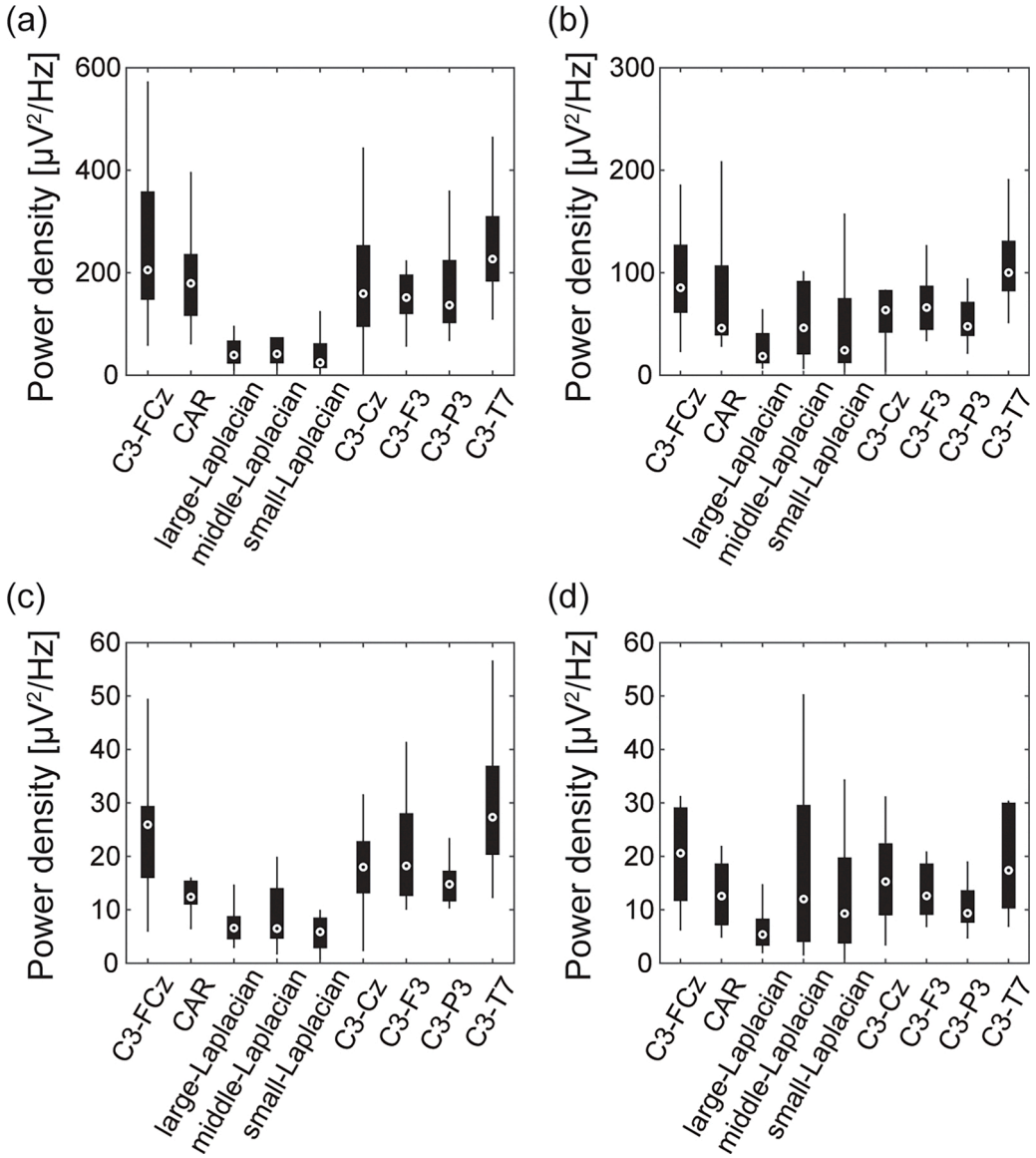

Fig. 1. Power density in each frequency band of EEG-SMR obtained after each spatial-filtering method applied.
Each panel depicts the power density in each frequency band of EEG-SMR; (*a*) alpha, (*b*) beta1, (*c*) beta2, and (*d*) beta3. In each bar, the circle sign indicates the median, and the top and bottom edges of the bar indicate the 25th and 75th percentiles, respectively.

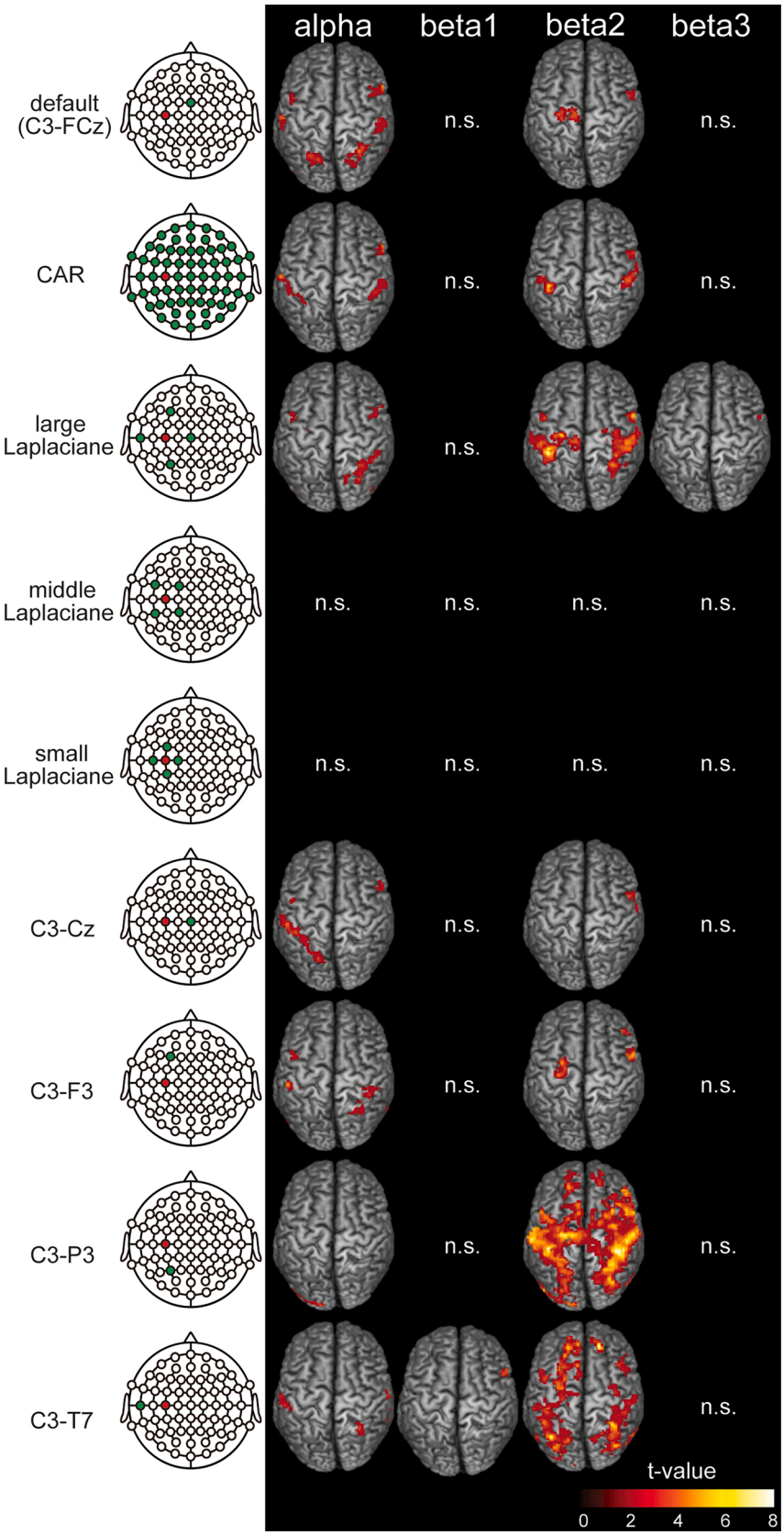

Fig. 2. Negative correlation maps in each frequency band of EEG-SMR obtained after each spatial-filtering method applied.
(*left*) The various spatial filters used, in which the red channel is in the C3 position and the green channels are the reference positions; each EEG-SMR is obtained by subtracting the averaged signal of the green channels from that in the C3 channel.
(*right*) The negative correlation maps between each spatial-filtered EEG-SMR and fMRI signal ($p < 0.001$ peak level uncorrected; $p = 0.05$ cluster-level FWE corrected). n.s.: not significant.

the lateral ventricles mask, which were anatomically defined by the SPM12 atlas. In the first-level analysis, we generated regression coefficient contrast images of each EEG-SMR power time course for each participant. For the second-level, group data analysis, the contrast images were fed into a one-sample t-test, resulting in the t-contrast images. For all data, the fMRI results were subjected to peak- and cluster-extent-based thresholding; the initial voxel threshold was set to $p < 0.001$, uncorrected for multiple comparisons, and the survived cluster threshold was set to $p < 0.05$ family-wise error (FWE) corrected for multiple comparisons for statistical inference.

Because there is functional connectivity between the left and right sensorimotor cortices in the resting-state (i.e., the sensorimotor network; Biswal et al., 1995), the EEG-SMR elicited from the C3 might reflect both of these activities (provided that we were able to successfully extract the left sensorimotor cortical activity via EEG-SMR spatial-filtering). Therefore, we defined the bilateral sensorimotor cortices as the target region from which activity was to be extracted via EEG-SMR spatial-filtering. The sensorimotor cortices were anatomically defined by pre/post central gyri in the automated anatomical labeling atlas 3 (AAL3, Rolls et al., 2020). Focusing on the negative correlation map of the alpha-band EEG-SMR, we calculated the number of statistically significant voxels in the sensorimotor cortices and the visual cortices that were also anatomically defined by occipital regions in AAL3. Furthermore, we used the negative correlation map of the alpha- and beta2-band EEG-SMRs to examine the relationship between the proportion of voxels that were significant in the sensorimotor cortices and the occupancy of sensorimotor cortices in all significant regions. The occupancy was obtained from the number of significant voxels in the sensorimotor cortices divided by the number of all significant voxels.

3. Results

Fig. 2 depicts the negative correlation maps of each spatial-filtered EEG-SMR and fMRI signal ($p < 0.001$ peak level uncorrected; $p = 0.05$ cluster-level FWE corrected). The maps of the alpha- and beta2-band EEG-SMR power time courses correlated mainly with the bilateral sensorimotor cortices, as opposed to those of the beta1- or beta3-band EEG-SMRs in most spatial-filters. Tables 1 and 2 show the alpha- and beta-bands EEG-SMRs correlation coordinates of the statistical maximum within the sensorimotor area and its cluster size. Following the Laplacian montage methods, the EEG-SMR resulting from the large-Laplacian filter was found to be more effective at reflecting the sensorimotor cortex than either the small- or middle-Laplacian. On the other hand, there was no significant region that was positively correlated with EEG-SMRs with any of the spatial-filtering methods. Fig. 3 depicts the relationship between the number of statistically significant voxels in the sensorimotor cortex and the visual cortex. The large-Laplacian and C3-F3 spatial-filters for the alpha-band EEG-SMR reflect the specific activity in the sensorimotor cortex, avoiding the activities derived from the visual cortex.

We further examined the relationship between the proportion of statistically significant voxels in the bilateral sensorimotor cortices and the ratio of the number of significant voxels in the sensorimotor cortices to the total significant voxels (Fig. 4). The beta2-band EEG-SMRs of the proportion of statistically significant voxels in the sensorimotor cortices was higher than that of the alpha-band EEG-SMRs in all spatial-filtering

Table 1
Brain regions whose activity correlated with the power of the alpha-band EEG-SMR obtained by each spatial-filtering method.

	Spatial-filter	Group-level statistical results							Sides	Atlas
		Cluster-level		Voxel-level (peak)						
		$P_{FWE\text{-}corr}$	Size	P_{uncorr}	t-score	MNI Coordinates				
alpha	a default reference (C3 - FCz)	2.6×10^{-2}	185	1.4×10^{-5}	5.56	−42	−2	32	Left	PrG
		7.2×10^{-4}	375	1.5×10^{-5}	5.54	58	18	18	Right	OpIFG
		2.2×10^{-2}	193	2.3×10^{-5}	5.33	−60	−18	28	Left	PoG
		8.5×10^{-5}	506	2.6×10^{-5}	5.27	30	−58	56	Right	SPL
		2.7×10^{-3}	300	6.1×10^{-5}	4.87	−18	−66	68	Left	SPL
		2.3×10^{-2}	191	1.2×10^{-4}	4.56	60	−46	0	Right	MTG
		2.5×10^{-2}	188	1.4×10^{-4}	4.51	54	−22	58	Right	PoG
		2.8×10^{-2}	183	3.7×10^{-4}	4.05	−42	−78	−4	Left	IOG
	CAR	4.8×10^{-3}	272	1.6×10^{-5}	5.51	−62	−16	28	Left	PoG
		3.8×10^{-2}	169	3.0×10^{-5}	5.20	58	18	18	Right	OpIFG
		3.2×10^{-2}	177	7.0×10^{-5}	4.81	50	−48	2	Right	MTG
		9.9×10^{-3}	234	1.3×10^{-4}	4.53	50	−34	48	Right	SMG
		5.5×10^{-3}	285	2.1×10^{-5}	5.38	−44	0	34	Left	PrG
		5.8×10^{-3}	282	3.4×10^{-5}	5.14	−42	−78	−14	Left	IOG
	large-Laplacian	1.2×10^{-4}	529	3.5×10^{-5}	5.13	40	16	34	Right	MFG
		1.7×10^{-4}	506	5.8×10^{-5}	4.90	30	−66	46	Right	SPL
		4.3×10^{-2}	175	9.8×10^{-5}	4.66	42	−78	12	RIght	MOG
	middle-Laplacian	–	–	–	–	–	–	–	–	–
	small-Laplacian	–	–	–	–	–	–	–	–	–
	C3 - Cz	2.3×10^{-2}	200	1.8×10^{-6}	6.55	−42	−2	32	Left	PrG
		1.2×10^{-6}	848	1.3×10^{-5}	5.61	−56	−28	50	Left	SMG
		1.8×10^{-2}	211	8.7×10^{-5}	4.71	54	−48	−2	Right	MTG
		1.8×10^{-2}	212	1.0×10^{-4}	4.63	56	14	18	Right	OpIFG
		1.1×10^{-3}	366	1.3×10^{-4}	4.51	−42	−76	−6	Left	IOG
		2.3×10^{-2}	220	2.8×10^{-5}	5.23	60	−16	22	Right	PoG
	C3 - F3	4.8×10^{-2}	180	3.9×10^{-5}	5.08	28	−54	56	Right	SPL
		2.7×10^{-2}	211	1.2×10^{-4}	4.58	−58	−28	48	Left	SMG
	C3 – P3	1.1×10^{-4}	587	1.4×10^{-5}	5.56	−38	−74	−10	Left	IOG
		2.8×10^{-5}	560	4.9×10^{-6}	6.07	−38	−72	−12	Left	OFug
		2.5×10^{-2}	183	1.2×10^{-5}	5.65	−54	−28	50	Left	PoG
	C3 – T7	9.1×10^{-3}	230	3.1×10^{-5}	5.19	48	−68	−4	Right	IOG
		2.2×10^{-3}	302	5.4×10^{-5}	4.93	32	−46	42	Right	SPL
		1.7×10^{-2}	200	6.5×10^{-5}	4.84	−46	0	36	Left	PrG

Brain regions are named based on the SPM12 atlas. CAR: common average reference; MNI : Montreal Neurological Institute; IOG: inferior occipital gyrus; MFG: middle frontal gyrus; MOG: middle occipital gyrus; MTG: middle temporal gyrus; OFuG: occipital fusiform gyrus; OpIFG: opercular part of the inferior frontal gyrus; PoG: postcentral gyrus; PrG: precentral gyrus; SMG: supramarginal gyrus; SPL: superior parietal lobule.

Table 2
Brain regions whose activity correlated with the power of the beta2-band EEG-SMR obtained by each spatial-filtering method.

	Spatial-filter	Group-level statistical results							Sides	Atlas
		Cluster-level		Voxel-level (peak)						
		$P_{FWE\text{-}corr}$	Size	P_{uncorr}	t-score	MNI Coordinates				
beta1	C3 - P3	2.7×10^{-2}	177	1.0×10^{-5}	5.72	38	18	30	Right	MFG
	a default reference; C3 - FCz	3.2×10^{-4}	495	9.3×10^{-6}	5.76	50	−2	14	Right	CO
		7.6×10^{-3}	285	3.7×10^{-5}	5.11	−12	−16	76	Left	PrG
		1.2×10^{-2}	381	1.3×10^{-7}	7.95	−40	−34	50	Left	PoG
	CAR	2.5×10^{-4}	486	2.0×10^{-5}	5.38	50	0	28	Right	PrG
		2.5×10^{-3}	336	2.7×10^{-5}	5.26	52	−24	46	Right	SMG
		6.0×10^{-11}	1817	8.0×10^{-9}	9.62	−40	−36	50	Left	PoG
		7.1×10^{-13}	2304	2.0×10^{-6}	6.50	44	2	32	Right	PrG
	large-Laplacian	2.4×10^{-2}	205	2.0×10^{-5}	5.49	−54	−40	−4	Left	MTG
		1.8×10^{-2}	221	4.0×10^{-5}	5.06	−48	0	34	Left	PrG
		2.1×10^{-2}	212	6.8×10^{-5}	4.83	−48	−72	−12	Left	IOG
	middle-Laplacian	–	–	–	–	–	–	–	–	–
	small-Laplacian	–	–	–	–	–	–	–	–	–
	C3 - Cz	1.1×10^{-9}	439	6.4×10^{-6}	8.80	46	0	30	Right	PrG
	C3 - F3	5.5×10^{-6}	865	8.1×10^{-6}	5.82	58	6	32	Right	PrG
		1.3×10^{-2}	267	1.4×10^{-5}	5.57	−26	−2	70	Left	SFG
beta2		$< 1.0 \times 10^{-14}$	27,054	1.0×10^{-7}	8.11	40	−36	62	Right	PoG
	C3 - P3	9.9×10^{-4}	337	6.9×10^{-6}	5.90	32	22	−8	Right	AIns
		1.8×10^{-3}	272	1.1×10^{-5}	5.68	−18	42	46	Left	SFG
		3.9×10^{-2}	159	5.9×10^{-5}	4.89	20	46	46	Right	SFG
		8.2×10^{-2}	217	1.4×10^{-7}	7.91	18	42	46	Right	SFg
		3.5×10^{-14}	2121	5.4×10^{-7}	7.19	−38	−66	48	Left	AnG
		$< 1.0 \times 10^{-14}$	3418	1.5×10^{-6}	6.65	36	−52	52	Right	SPL
		7.7×10^{-6}	591	2.6×10^{-6}	6.38	−22	−86	16	Left	SOG
		1.8×10^{-9}	1178	4.5×10^{-6}	6.11	−18	40	46	Left	SFG
	C3 - T7	2.2×10^{-3}	277	7.1×10^{-6}	5.89	32	24	−6	Right	AIns
		3.6×10^{-8}	953	7.2×10^{-6}	5.88	36	16	36	Right	MFG
		3.8×10^{-3}	252	1.4×10^{-5}	5.57	28	−44	−22	Right	FuG
		8.9×10^{-9}	1057	7.7×10^{-6}	5.50	−22	−62	−16	Left	IOG
		1.2×10^{-4}	430	1.7×10^{-5}	5.47	−38	10	30	Left	MFG
		1.1×10^{-2}	205	5.7×10^{-5}	4.90	−52	−64	18	Left	AnG
		3.9×10^{-2}	151	7.4×10^{-5}	4.78	−24	−20	70	Left	PrG
beta3	large-Laplacian	4.9×10^{-2}	198	5.3×10^{-5}	4.94	54	6	24	Right	PrG

Brain regions are named based on the SPM12 atlas. CAR: common average reference; MNI : Montreal Neurological Institute; AIns: anterior insula; AnG: angular gyrus; CO: central operculum; FuG: fusiform gyrus; IOG: inferior occipital gyrus; MFG: middle frontal gyrus; MTG: middle temporal gyrus; PoG: postcentral gyrus; PrG: precentral gyrus; SFG: superior frontal gyrus; SMG: supramarginal gyrus; SOG: superior occipital gyrus; SPL: superior parietal lobule.

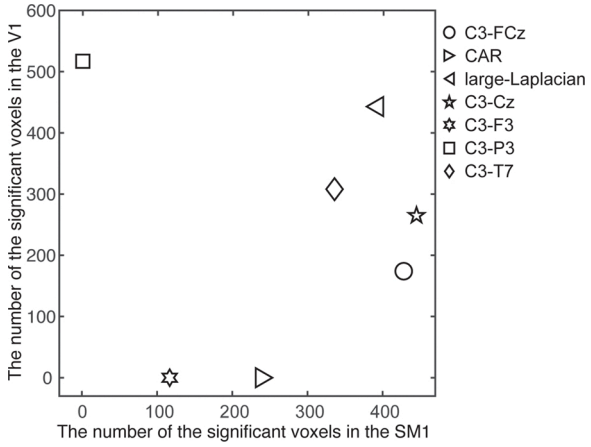

Fig. 3. Relationship between the number of significant voxels in the SM1 and V1 in the negative correlation map of the alpha-band EEG-SMR. The SM1 and V1 were anatomically defined by AAL3. SM1: sensorimotor cortex, V1: visual cortex, AAL3: automated anatomical labeling atlas 3.

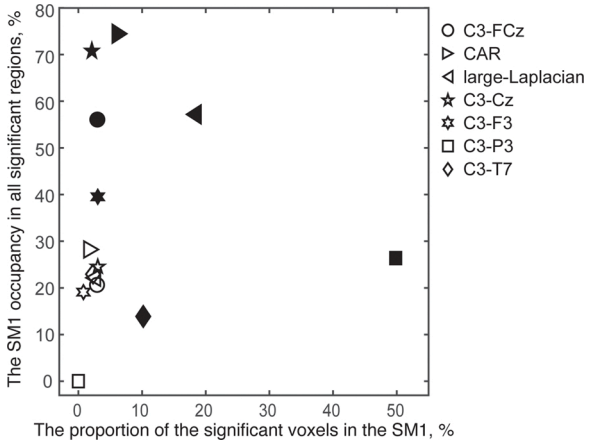

Fig. 4. The proportion of significant voxels in the SM1 and the SM1 occupancy of all significant regions. The proportion was obtained by the number of significant voxels divided by the total voxels in the bilateral sensorimotor cortices (SM1). The SM1 occupancy was calculated from the number of significant voxels in the SM1 divided by the number of all significant voxels in the whole-brain (White: the alpha-band EEG-SMR, Black: the beta2-band EEG-SMR).

methods. In addition, the sensorimotor occupancy in all significant regions in the beta2-band was higher than that of the alpha-band, and was particularly remarkable in the C3-P3 spatial-filtering method. The C3-P3 filtered beta2-band EEG-SMR correlated with many voxels, not only in the sensorimotor cortex, but also in other regions; thus, the specificity was very low. In this study, a higher number of sensorimotor cortex key voxels and a lower number of visual cortex key voxels represented potential predictors of a better filter to identify specific activities of the sensorimotor cortex. Therefore, the CAR spatial-filtering in alpha-band EEG-SMR extracted specific activity in the sensorimotor cortex. The

large-Laplacian spatial-filtering in beta2-band EEG-SMR provided adequate high specificity and sensitivity to extract the sensorimotor activities.

4. Discussion

Our simultaneous EEG-fMRI recordings demonstrated that using an average of signals over the whole brain (i.e., the CAR filter) as a reference for the signal of the C3 electrode was superior to other common spatial-filtering methods for extracting the alpha-band EEG-SMR, which reflects the sensorimotor activity. In the beta2-band EEG-SMR, the CAR also provided high specificity and the large-Laplacian provided adequate high specificity and sensitivity to extract the sensorimotor activity.

Our results indicated that the effectiveness of spatial-filtering to derive the EEG-SMR varied depending on the frequency of the oscillations. Although both the alpha- and beta-band EEG-SMR power modulations correlated with sensorimotor cortical activity, their frequency components were related to specific brain functions or regions (Angelini et al., 2018; Meirovitch et al., 2015; Pfurtscheller and Solis-Escalante, 2009; van Ede et al., 2014). It is well-known that the thalamus generates the alpha rhythm and also modulates cortical activity via the thalamocortical network (Hughes and Crunelli, 2005; Schreckenberger et al., 2004). Because the thalamus is a part of the sensory pathway (Herrero et al., 2002), the alpha rhythm can be recorded over many regions, including the sensorimotor cortex and the occipital cortex (Foxe and Snyder, 2011; Haegens et al., 2015; Pineda, 2005). The high-voltage alpha rhythm recorded over the occipital cortex when the eyes are closed is attenuated when the eyes are opened (Ben-Simon et al., 2013). In contrast, the alpha-band EEG-SMR power is not associated with visual stimulation (Geller et al., 2014), but its power is attenuated by proprioceptive sensory stimulation, such as haptic or electrical stimulation (Babiloni et al., 2008). In addition, the beta rhythm is more often found in the frontal or central areas than in the posterior regions of the cortex (Alegre et al., 2004). The most well-known beta rhythm is the basal ganglia oscillation, which is synchronous with oscillations in the cortical motor areas and reflected in the scalp-recorded beta rhythm (Kozelka and Pedley, 1990). Therefore, it is important for the spatial-filtering method in each frequency band EEG-SMR to distinguish and extract the specific activity of the sensorimotor cortex from the activity of the non-sensory motor area.

In the present study, the EEG-SMR obtained by smaller Laplacian montage filters were less effective at reflecting sensorimotor activity compared to the large-Laplacian. Because the Laplacian montages emphasize localized activity over the cortical electrical potential under the referenced electrodes (Le et al., 1994), the EEG component reflected the sensorimotor activity moderately distributed around the C3 area. As the distance of the referencing electrodes from the C3 decreases, the Laplacian filter becomes more sensitive to local electrical potentials with higher spatial frequencies and less sensitive to those with lower spatial frequencies (Hindriks et al., 2016). Because the alpha-band oscillations, such as occipital alpha, are widely distributed, the large-Laplacian are sufficient to improve the signal-to-noise ratios for extracting sensorimotor activity from the EEG-SMR signal. Similarly, the CAR spatial-filtering also extracts local activity in the sensorimotor cortex.

Our results also provided evidence for the usefulness of the bipolar spatial-filtering methods empirically used in clinical assessments (Benbadis, 2005; Kozelka and Pedley, 1990). The differences in the negative correlation maps of signals resulting from the four bipolar filters might be related to the cortical structures in the pericentral gyrus. Blankertz and colleagues (2010) reported differences in the distribution of signals depending on the electrical source locations in the gyri and sulci (Blankertz et al., 2010). Although fewer reference electrodes might be sensitive to electrode location relative to cortical structure, it is practical adopt an easy method to measure sensorimotor activity, especially for clinical assessment or EEG-SMR-based BCI applications. The present results showed that the forward or lateral bipolar montages (FCz, F3, Cz, and T7) were competent as reference electrodes at extracting sensorimotor activity, as they are located over the premotor or motor cortex. The referenced electrode set over the motor-related region might reflect the local activity within the sensorimotor cortex.

The present evaluation is significant for the construction of the BCI systems, especially concerning whether a particular biomarker reflects the desired activity in the brain region. For example, advances in machine learning and artificial intelligence have substantially enhanced BCI capabilities and their ability to classify the signals reflecting participants' intentions (Craik et al., 2019). On the other hand, in a motor exercise paradigm involving EEG-SMR-based BCI intervention to facilitate the enhancement of ipsilesional sensorimotor activity in post-stroke hemiplegic patients, even when high classification accuracy is provided by machine learning, if the feature does not reflect the ipsilesional sensorimotor activity, such a BCI intervention might be less effective (Ushiba and Soekadar, 2016). To aid motor function recovery with motor exercise contingent on the brain activity, it is crucial to construct an EEG-SMR-based BCI system that accurately reflects the sensorimotor activity (Clausen et al., 2017). In that sense, our study has provided more information about optimizing spatial-filtering methods for BCI interventions with high sensitivity and specificity that are capable of inducing beneficial motor function recovery.

Although current source estimation methods such as SimNibs and sLORETA, have been evaluated for how the electric field is formed when the reference montage is changed, the current sources estimation is poor with less than 64 channels and needs to be increased in density with more channels to improve the source estimation (Song et al., 2015; Sohrabpour et al., 2015). Besides, the current sources estimation has limitations in the evaluating spatial filters for EEG measurements due to the absence of the ground truth such as the more sources are present (Bradley et al., 2016). Hence, referring to the previous studies have already found that SMRs spontaneously oscillating at rest correlate with SM1 (Tsuchimoto et al., 2017; Yin et al., 2016), which provides the relationship between EEG-SMRs and SM1 activation, the present study provided the quantitative evaluation method with sensitivity and specificity of each spatial-filtering. This allowed us to confirm the filter optimization based on other physiological data (fMRI), which had not been clearly understood by the current source estimation based on modeling and optimization. This actually turned out to be not so good for the empirically used Small- or Middle-Laplacian and others. Those findings would be of potential importance to improve the existing spatial-filtering methods.

Our studies had several limitations. First, while we identified the brain region that correlated with EEG-SMRs obtained by commonly used spatial-filtering methods that employ simple combinations, we did not evaluate other spatial-filtering patterns based on weighted measures of several electrodes, such as common spatial pattern analysis. Although our results did show that the 63-channel CAR spatial-filtering method for alpha-band EEG-SMR was superior to other simpler methods, we did not evaluate the optimal number of electrodes needed to construct the CAR filter. Second, we did not yet consider other components, such as covariance with the alpha or beta rhythm. Although one may claim that the EEG-SMR component should be extracted via independent component analysis, this is a delicate procedure to set the number of independent components in which the maximum number depends on the number of electrodes, and to confirm that these separate components reflect sensorimotor cortical activity when using the EEG-SMR application in BCIs or clinical assessments. Third, although other researchers performing recent fMRI data analysis did not apply spatial smoothing (Coalson et al., 2018; Gardumi et al., 2016; Glasser et al., 2013), we applied the spatial smoothing of 4 mm FWHM that was as large as the fMRI original voxel size, compensating for imperfect registration in spatial normalization across participants and for individual differences in neural organization. This spatial smoothing processing decreases high spatial frequency noises but also increased the spatial bias (i.e. partial

volume effect) of true signals and structure noises (Coalson et al., 2018). To identify the precise region within the sensorimotor cortex that correlated with EEG-SMR, the fMRI data with high contrast and structural images are needed. In addition, it is subtle that all voxels in the sensorimotor region are correlated with EEG-SMR. Considering the spatial resolution of EEG, it cannot be assumed that an extremely restricted area correlated with EEG-SMR. If so, EEG-SMR resulting from the small-Laplacian filter would better reflect the sensorimotor cortical activity than the middle- or large-Laplacian. Finally, we evaluate the spatial-filtering for EEG-SMR focusing on the relationships between the EEG-SMR and SM1 BOLD activity, but we did not examine the relationship between the spatial-filtering of EEG-SMR and whole-brain connectivity. Whole-brain connectivity during resting state has been commonly studied metric and further studies will be warranted to reveal how these different reference methods would affect the correlation/similarity of connectivity pattern between EEG and fMRI. In this study, we evaluated relatively simple methods for spatial-filtering to extract intrinsic activity; further studies are required to identify the optimal spatial-filters for these and other activities.

5. Conclusions

Using simultaneous EEG-fMRI recordings in the resting state to evaluate the spatial-filtering methods commonly used for extracting sensorimotor activity from the EEG-SMR, we demonstrated that the CAR, an average of reference signals from the whole brain, and large-Laplacian filters provided higher sensitivity and specificity than did the seven other filters examined. We suggest this as a useful procedure to follow in order to more effectively construct EEG-SMR-based BCI interventions. Furthermore, we expect that our method can be applied not only to identify the optimal spatial-filter for EEG-SMR, but also to identify novel spatial-filters for extracting activities in brain regions other than the sensorimotor cortex and thus lead to new insights into the intrinsic oscillations responsible for EEG signals.

CRediT authorship contribution statement

Shohei Tsuchimoto: Conceptualization, Data curation, Formal analysis, Investigation, Methodology, Resources, Software, Validation, Visualization, Writing - original draft, Writing - review & editing. **Shuka Shibusawa:** Conceptualization, Data curation, Investigation, Methodology, Resources, Validation, Writing - original draft, Writing - review & editing. **Seitaro Iwama:** Conceptualization, Data curation, Formal analysis, Methodology, Software, Validation, Visualization, Writing - original draft, Writing - review & editing. **Masaaki Hayashi:** Conceptualization, Data curation, Resources, Validation, Writing - original draft, Writing - review & editing. **Kohei Okuyama:** Conceptualization, Data curation, Resources, Validation, Writing - original draft, Writing - review & editing. **Nobuaki Mizuguchi:** Conceptualization, Data curation, Formal analysis, Methodology, Validation, Visualization, Writing - original draft, Writing - review & editing. **Kenji Kato:** Conceptualization, Data curation, Investigation, Methodology, Resources, Validation, Writing - original draft, Writing - review & editing. **Junichi Ushiba:** Conceptualization, Funding acquisition, Project administration, Supervision, Writing - original draft, Writing - review & editing.

Declaration of Competing Interest

J.U. is one of the founders and the Representative Director of the University Startup Company, Connect Inc. for the research, development, and sales of rehabilitation devices including brain-computer interface. J.U. has received a salary from Connect Inc., and has held the shares of Connect Inc. This company does not have any relationship with the present study.

Acknowledgement

This work was partly supported by Grant-in-Aid for Scientific Research (C) (JP16K01469), Grant-in-Aid for Young Scientists (B) (JP25750267), and the Japan Agency for Medical Research and Development (AMED) (JP20he2302006). We thank Kumi Nanjo and Sayoko Ishii for their technical supports.

References

Alegre, M., Gurtubay, I.G., Labarga, A., Iriarte, J., Valencia, M., Artieda, J., 2004. Frontal and central oscillatory changes related to different aspects of the motor process: a study in go/no-go paradigms. Exp. Brain Res. 159, 14–22. https://doi.org/10.1007/s00221-004-1928-8.

Allen, P.J., Josephs, O., Turner, R., 2000. A method for removing imaging artifact from continuous EEG recorded during functional MRI. Neuroimage 12, 230–239. https://doi.org/10.1006/nimg.2000.0599.

Angelini, M., Fabbri-Destro, M., Lopomo, N.F., Gobbo, M., Rizzolatti, G., Avanzini, P., 2018. Perspective-dependent reactivity of sensorimotor mu rhythm in alpha and beta ranges during action observation: an EEG study. Sci. Rep. 8, 12429. https://doi.org/10.1038/s41598-018-30912-w.

Arroyo, S., Lesser, R.P., Gordon, B., Uematsu, S., Jackson, D., Webber, R., 1993. Functional significance of the mu rhythm of human cortex: an electrophysiologic study with subdural electrodes. Electroencephalogr. Clin. Neurophysiol. 87, 76–87. https://doi.org/10.1016/0013-4694(93)90114-B.

Babiloni, C., Capotosto, P., Brancucci, A., Del Percio, C., Petrini, L., Buttiglione, M., Cibelli, G., Romani, G.L., Rossini, P.M., Arendt-Nielsen, L., 2008. Cortical alpha rhythms are related to the anticipation of sensorimotor interaction between painful stimuli and movements: a high-resolution EEG study. J. Pain 9, 902–911. https://doi.org/10.1016/j.jpain.2008.05.007.

Benbadis, S.R., 2005. Introduction to sleep electroencephalography. Sleep: A Comprehensive Handbook, pp. 989–1024. https://doi.org/10.1002/0471751723.ch130.

Ben-Simon, E., Podlipsky, I., Okon-Singer, H., Gruberger, M., Cvetkovic, D., Intrator, N., Hendler, T., 2013. The dark side of the alpha rhythm: fMRI evidence for induced alpha modulation during complete darkness. Eur. J. Neurosci. 37, 795–803. https://doi.org/10.1111/ejn.12083.

Biswal, B., Yetkin, F.Z., Haughton, V.M., Hyde, J.S., 1995. Functional connectivity in the motor cortex of resting human brain using echo-planar MRI. Magn. Reson. Med. 34, 537–541. https://doi.org/10.1002/mrm.1910340409.

Blankertz, B., Tomioka, R., Lemm, S., Kawanabe, M., Muller, K., 2008. Optimizing spatial filters for robust EEG single-trial analysis. IEEE Signal Process. Mag. 25, 41–56. https://doi.org/10.1109/MSP.2008.4408441.

Blankertz, B., Tangermann, M., Vidaurre, C., Fazli, S., Sannelli, C., Haufe, S., Maeder, C., Ramsey, L., Sturm, I., Curio, G., Müller, K.-R., 2010. The berlin brain–computer interface: non-medical uses of BCI technology. Front. Neurosci. 4, 17. https://doi.org/10.3389/fnins.2010.00198. Article ID 00198.

Bradley, A., Yao, J., Dewald, J., Richter, C.-P., 2016. Evaluation of electroencephalography source localization algorithms with multiple cortical sources. PLoS One 11. https://doi.org/10.1371/journal.pone.0147266.

Carter, A.R., Astafiev, S.V., Lang, C.E., Connor, L.T., Rengachary, J., Strube, M.J., Pope, D.L.W., Shulman, G.L., Corbetta, M., 2010. Resting inter-hemispheric fMRI connectivity predicts performance after stroke. Ann. Neurol. 67, 365–375. https://doi.org/10.1002/ana.21905.

Clausen, J., Fetz, E., Donoghue, J., Ushiba, J., Spörhase, U., Chandler, J., Birbaumer, N., Soekadar, S.R., 2017. Help, hope, and hype: Ethical dimensions of neuroprosthetics. Science 356, 1338–1339. https://doi.org/10.1126/science.aam7731.

Coalson, T.S., Essen, D.C.V., Glasser, M.F., 2018. The impact of traditional neuroimaging methods on the spatial localization of cortical areas. PNAS 115, E6356–E6365. https://doi.org/10.1073/pnas.1801582115.

Craik, A., He, Y., Contreras-Vidal, J.L., 2019. Deep learning for electroencephalogram (EEG) classification tasks: a review. J. Neural Eng. 16, 031001 https://doi.org/10.1088/1741-2552/ab0ab5.

Drysdale, A.T., Grosenick, L., Downar, J., Dunlop, K., Mansouri, F., Meng, Y., Fetcho, R.N., Zebley, B., Oathes, D.J., Etkin, A., Schatzberg, A.F., Sudheimer, K., Keller, J., Mayberg, H.S., Gunning, F.M., Alexopoulos, G.S., Fox, M.D., Pascual-Leone, A., Voss, H.U., Casey, B., Dubin, M.J., Liston, C., 2017. Resting-state connectivity biomarkers define neurophysiological subtypes of depression. Nat. Med. 23, 28–38. https://doi.org/10.1038/nm.4246.

Foxe, J.J., Snyder, A.C., 2011. The role of alpha-band brain oscillations as a sensory suppression mechanism during selective attentios. Front. Psychol. 2 https://doi.org/10.3389/fpsyg.2011.00154.

Gardumi, A., Ivanov, D., Hausfeld, L., Valente, G., Formisano, E., Uludağ, K., 2016. The effect of spatial resolution on decoding accuracy in fMRI multivariate pattern analysis. NeuroImage 132, 32–42. https://doi.org/10.1016/j.neuroimage.2016.02.033.

Geller, A.S., Burke, J.F., Sperling, M.R., Sharan, A.D., Litt, B., Baltuch, G.H., Lucas, T.H., Kahana, M.J., 2014. Eye closure causes widespread low-frequency power increase and focal gamma attenuation in the human electrocorticogram. Clin. Neurophysiol. 125, 1764–1773. https://doi.org/10.1016/j.clinph.2014.01.021.

Glasser, M.F., Sotiropoulos, S.N., Wilson, J.A., Coalson, T.S., Fischl, B., Andersson, J.L., Xu, J., Jbabdi, S., Webster, M., Polimeni, J.R., Van Essen, D.C., Jenkinson, M., WU-Minn HCP Consortium, 2013. The minimal preprocessing pipelines for the human

connectome project. Neuroimage 80, 105–124. https://doi.org/10.1016/j.neuroimage.2013.04.127.
Goldman, R.I., Stern, J.M., Engel, J., Cohen, M.S., 2000. Acquiring simultaneous EEG and functional MRI. Clin. Neurophysiol. 111, 1974–1980. https://doi.org/10.1016/S1388-2457(00)00456-9.
Haegens, S., Barczak, A., Musacchia, G., Lipton, M.L., Mehta, A.D., Lakatos, P., Schroeder, C.E., 2015. Laminar profile and physiology of the α rhythm in primary visual, auditory, and somatosensory regions of neocortex. J. Neurosci. 35, 14341–14352. https://doi.org/10.1523/JNEUROSCI.0600-15.2015.
Herrero, M.-T., Barcia, C., Navarro, J., 2002. Functional anatomy of thalamus and basal ganglia. Childs Nerv. Syst. 18, 386–404. https://doi.org/10.1007/s00381-002-0604-1.
Hindriks, R., Arsiwalla, X.D., Panagiotaropoulos, T., Besserve, M., Verschure, P.F.M.J., Logothetis, N.K., Deco, G., 2016. Discrepancies between multi-electrode LFP and CSD phase-patterns: a forward modeling study. Front. Neural Circuits 10. https://doi.org/10.3389/fncir.2016.00051.
Hjorth, B., 1991. Principles for transformation of scalp EEG from potential field into source distribution. J. Clin. Neurophysiol. 8, 391–396. https://doi.org/10.1097/00004691-199110000-00004.
Hughes, S.W., Crunelli, V., 2005. Thalamic mechanisms of EEG alpha rhythms and their pathological implications. Neuroscientist 11, 357–372. https://doi.org/10.1177/1073858405277450.
Jurcak, V., Tsuzuki, D., Dan, I., 2007. 10/20, 10/10, and 10/5 systems revisited: their validity as relative head-surface-based positioning systems. Neuroimage 34, 1600–1611. https://doi.org/10.1016/j.neuroimage.2006.09.024.
Kozelka, J.W., Pedley, T.A., 1990. Beta and mu rhythms. J. Clin. Neurophysiol. 7, 191–208. https://doi.org/10.1097/00004691-199004000-00004.
Krishnaswamy, P., Obregon-Henao, G., Ahveninen, J., Khan, S., Babadi, B., Iglesias, J.E., Hämäläinen, M.S., Purdon, P.L., 2017. Sparsity enables estimation of both subcortical and cortical activity from MEG and EEG. PNAS 114, E10465–E10474. https://doi.org/10.1073/pnas.1705414114.
Le, J., Menon, V., Gevins, A., 1994. Local estimate of surface Laplacian derivation on a realistically shaped scalp surface and its performance on noisy data. Electroencephalogr. Clin. Neurophysiol. Potentials Sect. 92, 433–441. https://doi.org/10.1016/0168-5597(94)90021-3.
McFarland, D.J., McCane, L.M., David, S.V., Wolpaw, J.R., 1997. Spatial filter selection for EEG-based communication. Electroencephalogr. Clin. Neurophysiol. 103, 386–394. https://doi.org/10.1016/S0013-4694(97)00022-2.
Meirovitch, Y., Harris, H., Dayan, E., Arieli, A., Flash, T., 2015. Alpha and beta band event-related desynchronization reflects kinematic regularities. J. Neurosci. 35, 1627–1637. https://doi.org/10.1523/JNEUROSCI.5371-13.2015.
Moon, J.-Y., Kim, J., Ko, T.-W., Kim, M., Iturria-Medina, Y., Choi, J.-H., Lee, J., Mashour, G.A., Lee, U., 2017. Structure shapes dynamics and directionality in diverse brain networks: mathematical principles and empirical confirmation in three species. Sci. Rep. 7, 46606. https://doi.org/10.1038/srep46606.
Neuper, C., Wörtz, M., Pfurtscheller, G., 2006. ERD/ERS patterns reflecting sensorimotor activation and deactivation. Prog. Brain Res. Event-Related Dyn. Brain Oscillations 159, 211–222. https://doi.org/10.1016/S0079-6123(06)59014-4.
Pfurtscheller, G., Aranibar, A., 1977. Event-related cortical desynchronization detected by power measurements of scalp EEG. Electroencephalogr. Clin. Neurophysiol. 42, 817–826. https://doi.org/10.1016/0013-4694(77)90235-8.
Pfurtscheller, G., Solis-Escalante, T., 2009. Could the beta rebound in the EEG be suitable to realize a “brain switch”? Clin. Neurophysiol. 120, 24–29. https://doi.org/10.1016/j.clinph.2008.09.027.
Pfurtscheller, G., Brunner, C., Schlögl, A., Lopes da Silva, F.H., 2006. Mu rhythm (de) synchronization and EEG single-trial classification of different motor imagery tasks. Neuroimage 31, 153–159. https://doi.org/10.1016/j.neuroimage.2005.12.003.
Pineda, J.A., 2005. The functional significance of mu rhythms: translating “seeing” and “hearing” into “doing.”. Brain Res. Rev. 50, 57–68. https://doi.org/10.1016/j.brainresrev.2005.04.005.
Power, J.D., Barnes, K.A., Snyder, A.Z., Schlaggar, B.L., Petersen, S.E., 2012. Spurious but systematic correlations in functional connectivity MRI networks arise from subject motion. Neuroimage 59, 2142–2154. https://doi.org/10.1016/j.neuroimage.2011.10.018.
Ramoser, H., Muller-Gerking, J., Pfurtscheller, G., 2000. Optimal spatial filtering of single trial EEG during imagined hand movement. Ieee Trans. Rehabil. Eng. 8, 441–446. https://doi.org/10.1109/86.895946.
Rangaswamy, M., Porjesz, B., Chorlian, D.B., Wang, K., Jones, K.A., Bauer, L.O., Rohrbaugh, J., O’Connor, S.J., Kuperman, S., Reich, T., Begleiter, H., 2002. Beta power in the EEG of alcoholics. Biol. Psychiatry 52, 831–842. https://doi.org/10.1016/S0006-3223(02)01362-8.
Rangaswamy, M., Porjesz, B., Chorlian, D.B., Wang, K., Jones, K.A., Kuperman, S., Rohrbaugh, J., O’Connor, S.J., Bauer, L.O., Reich, T., Begleiter, H., 2004. Resting EEG in offspring of male alcoholics: beta frequencies. Int. J. Psychophysiol. 51, 239–251. https://doi.org/10.1016/j.ijpsycho.2003.09.003.
Ritter, P., Villringer, A., 2006. Simultaneous EEG–fMRI. Neurosci. Biobehav. Rev., Methodol. Conceptual Adv. Study Brain-Behav. Dyn. A Multivar. Lifespan Perspect. 30, 823–838. https://doi.org/10.1016/j.neubiorev.2006.06.008.
Ritter, P., Moosmann, M., Villringer, A., 2009. Rolandic alpha and beta EEG rhythms’ strengths are inversely related to fMRI-BOLD signal in primary somatosensory and motor cortex. Hum. Brain Mapp. 30, 1168–1187. https://doi.org/10.1002/hbm.20585.
Rolls, E.T., Huang, C.-C., Lin, C.-P., Feng, J., Joliot, M., 2020. Automated anatomical labelling atlas 3. Neuroimage 206, 116189. https://doi.org/10.1016/j.neuroimage.2019.116189.
Schreckenberger, M., Lange-Asschenfeld, C., Lochmann, M., Mann, K., Siessmeier, T., Buchholz, H.-G., Bartenstein, P., Gründer, G., 2004. The thalamus as the generator and modulator of EEG alpha rhythm: a combined PET/EEG study with lorazepam challenge in humans. Neuroimage 22, 637–644. https://doi.org/10.1016/j.neuroimage.2004.01.047.
Seeber, M., Cantonas, L.-M., Hoevels, M., Sesia, T., Visser-Vandewalle, V., Michel, C.M., 2019. Subcortical electrophysiological activity is detectable with high-density EEG source imaging. Nat. Commun. 10, 753. https://doi.org/10.1038/s41467-019-08725-w.
Sitaram, R., Ros, T., Stoeckel, L., Haller, S., Scharnowski, F., Lewis-Peacock, J., Weiskopf, N., Blefari, M.L., Rana, M., Oblak, E., Birbaumer, N., Sulzer, J., 2017. Closed-loop brain training: the science of neurofeedback. Nat. Rev. Neurosci. 18, 86–100. https://doi.org/10.1038/nrn.2016.164.
Sohrabpour, A., Lu, Y., Kankirawatana, P., Blount, J., Kim, H., He, B., 2015. Effect of EEG electrode number on epileptic source localization in pediatric patients. Clin. Neurophysiol. 126, 472–480. https://doi.org/10.1016/j.clinph.2014.05.038.
Song, J., Davey, C., Poulsen, C., Luu, P., Turovets, S., Anderson, E., Li, K., Tucker, D., 2015. EEG source localization: sensor density and head surface coverage. J. Neurosci. Methods 256, 9–21. https://doi.org/10.1016/j.jneumeth.2015.08.015.
Tsuchimoto, S., Shibusawa, S., Mizuguchi, N., Kato, K., Ebata, H., Liu, M., Hanakawa, T., Ushiba, J., 2017. Resting-state fluctuations of EEG sensorimotor rhythm reflect BOLD activities in the pericentral areas: a simultaneous EEG-fMRI study. Front. Hum. Neurosci. 11, 10. https://doi.org/10.3389/fnhum.2017.00356.
Ushiba, J., Soekadar, S.R., 2016. Brain–machine interfaces for rehabilitation of poststroke hemiplegia. Prog. Brain Res. Brain-Comput. Interfaces: Lab Exp. Real-World Appl. 228, 163–183. https://doi.org/10.1016/bs.pbr.2016.04.020.
Vahdat, S., Darainy, M., Milner, T.E., Ostry, D.J., 2011. Functionally specific changes in resting-state sensorimotor networks following motor learning. J. Neurosci. 31, 16907–16915. https://doi.org/10.1523/JNEUROSCI.2737-11.2011.
van Ede, F., Szebényi, S., Maris, E., 2014. Attentional modulations of somatosensory alpha, beta and gamma oscillations dissociate between anticipation and stimulus processing. Neuroimage 97, 134–141. https://doi.org/10.1016/j.neuroimage.2014.04.047.
Yin, S., Liu, Y., Ding, M., 2016. Amplitude of sensorimotor mu rhythm is correlated with BOLD from multiple brain regions: a simultaneous EEG-fMRI study. Front. Hum. Neurosci. 10. https://doi.org/10.3389/fnhum.2016.00364.
Zumer, J.M., Scheeringa, R., Schoffelen, J.-M., Norris, D.G., Jensen, O., 2014. Occipital alpha activity during stimulus processing gates the information flow to object-selective cortex. PLoS Biol. 12, e1001965 https://doi.org/10.1371/journal.pbio.1001965.